

# Chiral-Split Magnon in Altermagnetic MnTe

Zheyuan Liu,<sup>1</sup> Makoto Ozeki,<sup>1</sup> Shinichiro Asai,<sup>1</sup> Shinichi Itoh,<sup>2,3</sup> and Takatsugu Masuda<sup>1,2,4</sup>

<sup>1</sup>*Institute for Solid State Physics, the University of Tokyo, Kashiwa 277-8581, Japan*

<sup>2</sup>*Institute of Materials Structure Science, High Energy Accelerator Research Organization, Ibaraki 305-0801, Japan*

<sup>3</sup>*Materials and Life Science Division, J-PARC Center, Tokai, Ibaraki 319-1195, Japan*

<sup>4</sup>*Trans-scale Quantum Science Institute, The University of Tokyo, Tokyo 113-0033, Japan*

(Dated: August 30, 2024)

Altermagnetism is a newly discovered magnetic class named after the alternating spin polarizations in both real and reciprocal spaces. Like the spin-splitting of electronic bands, the magnon bands in altermagnets are predicted to exhibit alternating chiral splitting. In this work, by performing inelastic neutron scattering on  $\alpha$ -MnTe, we directly verified the chiral splitting in altermagnetic magnon dispersions. The lifted degeneracy of chirality is further explained by a symmetric-exchange origin. In addition, the  $g$ -wave magnetism was identified in MnTe.

Altermagnets have been recently categorized as a third elementary type of collinear magnetic phases in addition to the conventional ferromagnets and antiferromagnets [1, 2]. The distinct spin symmetries in altermagnets simultaneously keep the compensated spin arrangement and break the time-reversal symmetry (TRS). Consequently, electronic bands in altermagnets are spin-splitting even in the absence of the relativistic spin-orbit coupling. The unconventional spin-splitting has been predicted to be significant owing to the exchange origin [3–13], and has been subsequently observed in altermagnetic candidates MnTe [14–16], RuO<sub>2</sub> [17], and CrSb [18] by angle-resolved photoemission spectroscopy (ARPES). Besides the band splitting, altermagnets exhibit various exotic quantum phenomena related to the TRS breaking nature, such as the anomalous Hall effect [19–21], charge-spin current conversion [22–27], spin splitter torque [28, 29], magnetic circular dichroism [30], and piezomagnetic effect [25, 31]. These remarkable findings establish a firm foundation for the altermagnetic spintronics functionalities [1].

Similar to the spin-splitting of electronic bands, the altermagnetic magnons are theoretically predicted to exhibit chiral splitting within the consideration of symmetric exchange interactions [32, 33]. The spin current in ferromagnets carried by the chiral magnons is only operational at slow GHz rates due to the quadratic magnon dispersion. By contrast, the linear dispersive chiral magnons in altermagnets reach the THz frequencies, unveiling the potential for the stray-field-free ultra-fast spintronics [1, 32]. In this letter, we performed inelastic neutron scattering (INS) on altermagnetic MnTe single crystals. The non-degenerated magnon dispersions are unambiguously verified in the observed spectra. The obtained spin Hamiltonian demonstrates that the alternating superexchange interactions lift the magnon degeneracy for both energy and chirality. Our result provides the evidence for altermagnetic magnon chiral splitting and highlights the exchange origin of altermagnetic nature.

The studied material,  $\alpha$ -MnTe, hosts a centrosymmetric hexagonal lattice with a space group  $P6_3/mmc$ , as shown in Figs. 1(a) and 1(b). Below Néel temperature

$T_N = 307$  K, an  $A$ -type antiferromagnetic (AFM) ground state was realized where the spins  $S = 5/2$  of Mn<sup>2+</sup> ions are ferromagnetically orientated along the crystallographic  $b^*$ -axis in the  $ab$ -plane and antiferromagnetically arranged between adjacent layers [34–36]. The opposite-spin sublattices, Mn<sub>A</sub> and Mn<sub>B</sub>, are connected by a mirror operation or sixfold rotation instead of any translation or inversion, which meets the classification of altermagnets, as shown in Fig. 1(a). The mirror and sixfold rotation symmetries protect the degeneracy for electronic bands in four nodal planes (NPs) [14, 15], as shown in Fig. 1(c), in addition to the Brillouin zone (BZ) boundaries. The bulk-sensitive X-ray ARPES on MnTe revealed a half-eV-scale spin-splitting in the electronic bands off the NPs [14], suggesting a significant altermagnetic effect in MnTe.

Based on the spin symmetry, the altermagnetic superexchange interactions in MnTe are analyzed to be the tenth and eleventh nearest neighbor interactions,  $J_{10}$  and  $J_{11}$ , which alternatively connect the same-spin sublattices, as illustrated by the dashed curves in Fig. 1(b). Although the distanced interactions  $J_{10}$  and  $J_{11}$  are inevitably weak, they are expected to differ in value or even in sign because of the different exchange paths through the Te orbitals. Similar to the electronic bands, the degeneracy of the chiral magnons is found to be protected by the symmetries between the sublattices as well. Inside the NPs and BZ boundaries, the altermagnetic magnon dispersion is identical to the conventional AFM magnon dispersion, as illustrated by the dispersion along  $\Gamma - K$  shown in Fig. 1(d). However, a finite difference between  $J_{10}$  and  $J_{11}$  lifts the magnon degeneracy off the NPs and BZ boundaries, while the altermagnetic magnons still maintain the AFM-like linear dispersion near the  $\Gamma$ -point, as illustrated by the dispersions along  $\Gamma - L$  shown in Fig. 1(e). The constant-energy contour of the non-degenerated dispersions in the  $c^*$ -planes shows a  $g$ -wave harmonic symmetry in MnTe, as shown in Fig. 1(f). Note that these non-degenerated dispersions are alternating chiral-split as well. Previous INS experiments on MnTe limited by a relatively relaxed energy resolution only probed the first, second and third nearest neighbor

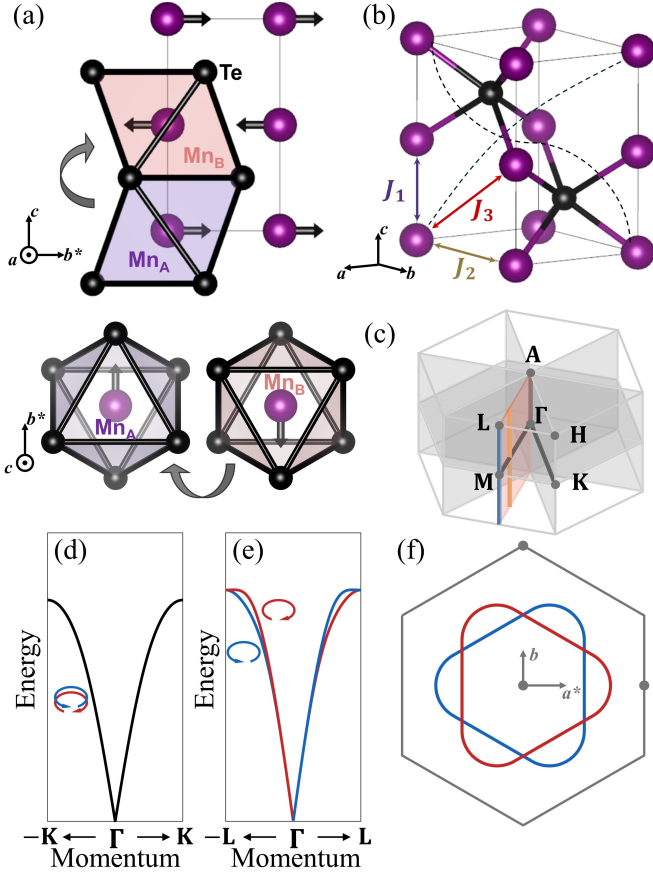


FIG. 1. (a) Lattice and spin structure of MnTe. The two opposite-spin sublattices,  $\text{Mn}_A$  and  $\text{Mn}_B$ , are connected by a real-space mirror or sixfold rotation symmetry. (b) Exchange paths between  $\text{Mn}^{2+}$  spins. The dashed curves highlight the altermagnetic superexchange paths. (c) Schematics of the MnTe BZ with four spin-degenerate NPs (in gray). The  $\Gamma$ MLA-plane is indicated in red. Schematics of altermagnetic magnon dispersion (d) in the NPs along  $\Gamma - \text{K}$  and (e) off the NPs along  $\Gamma - \text{L}$ . (f) The constant-energy contour of the altermagnetic magnon dispersions in a  $c^*$ -plane off the NPs and BZ boundaries.

exchange interactions (denoted as  $J_1$ ,  $J_2$ , and  $J_3$ ) [37], and would miss the splitting feature of the magnon dispersions.

To perform INS, large MnTe single crystals were synthesized by the self-flux method [38]. Five crystals with total mass of 4.2 g were co-aligned with a scattering plane spanned by  $(h, 0, 0)$  and  $(0, 0, l)$ . The INS experiments were carried on the High Resolution Chopper (HRC) spectrometer installed at BL-12 in MLF, J-PARC [39–41]. A Gifford-McMahon type cryostat was used for controlling the temperature. The frequency of Fermi chopper was 200 Hz. The incident energies,  $E_i$ s, of 50.8 meV and 11.4 meV were used for the measurements at  $T = 10$  K. HRC has vertical detector banks, thus accesses the momentum ( $Q$ ) space out of the scattering plane.

Well-defined magnon excitations were observed by the INS experiments with  $E_i = 50.8$  meV, as shown

in Fig. 2. The spectrum along high symmetric  $Q$ -paths,  $M'(-\frac{1}{2}, \frac{1}{2}, 1)$ - $\text{K}(-\frac{2}{3}, \frac{1}{3}, 1)$ - $\Gamma(-1, 0, 1)$ - $\text{M}(-\frac{3}{2}, 0, 1)$ - $\text{L}(-\frac{3}{2}, 0, \frac{3}{2})$ - $\text{A}(-1, 0, \frac{3}{2})$ - $\Gamma(-1, 0, 1)$ - $\text{H}(-\frac{1}{2}, \frac{1}{2}, \frac{3}{2})$ , which are all inside the spin-degenerate NPs, is shown in Fig. 2(a). It presents a typical AFM-like magnon dispersions with a single-ion easy-plane anisotropy. The spots around  $E = 5$  meV at K and M points are considered as artifacts, since they are absent in the spectrum with  $E_i = 11.4$  meV. In contrast to the spectrum in the NPs, the dispersions off the NPs and BZ boundaries are distinct from the AFM magnon dispersions. Spectrum along  $\Gamma(-1, 0, 1)$ - $\text{L}(-\frac{1}{2}, 0, \frac{3}{2})$  in Fig. 2(b) shows a magnon splitting above  $E \sim 30$  meV, while the dispersions keep the linear feature in the lower energy range. This splitting gradually smears when approaching  $\Gamma$  or L in the spin-degenerate NP. The split dispersions were clearly observed along the  $(-1.33, 0, l)$  direction, as shown in Fig. 2(d). The two non-degenerated magnon modes alternatively propagate along the  $c^*$ -axis, forming nodal points at integer and half-integer  $l$ , which implies the mirror symmetry of the  $\text{Mn}^{2+}$  sublattices. For comparison, we present a similar dispersion along  $(-1.5, 0, l)$  in the BZ boundary, as shown in Fig. 2(g). The one-dimensional (1-D) constant- $Q$  cuts of the split dispersions along  $(-1.33, 0, l)$  in Fig. 2(i) demonstrate a double-peak splitting of 2 meV in most of the intermediate  $l$  range ( $-1 < l < -1.5$ ). In contrast, at  $l = -1$ ,  $-1.5$  and every cut along  $(-1.5, 0, l)$  in Fig. 2(j), the excitation is a sharp single peak.

The  $g$ -wave harmonic symmetry of the altermagnetic MnTe which originates from the improper sixfold rotation between the  $\text{Mn}^{2+}$  sublattices [1, 2] was unambiguously verified in the constant- $E$  slice in the off-nodal  $(h, k, -1.33)$ -plane, as shown in Figs. 3(a)- 3(c). The sixfold high intensity nodal points were clearly observed at  $E = 33$  meV to 34 meV. The split contour of the dispersion shows a typical intertwined  $g$ -wave pattern, again relating the unconventional splitting to the spin symmetry.

To identify the spin Hamiltonian, calculations were performed based on the linear spin-wave theory (LSWT) by using SpinW package [42]. Because the concept of altermagnetism is within the category of symmetric exchange interaction, we consider a Heisenberg spin Hamiltonian with a single-ion easy-plane anisotropy, represented by

$$\mathcal{H} = \sum_{\langle i, j \rangle} J_{ij} \mathbf{S}_i \cdot \mathbf{S}_j + \sum_i D(S_i^z)^2, \quad (1)$$

where  $i$  denotes the index of  $\text{Mn}^{2+}$  spin and  $\mathbf{S}_i$  is the spin operator.  $J_{ij}$  is the exchange interactions between  $i$ th and  $j$ th spins. The sum is taken over pairs of spins.  $D$  is the anisotropy constant, and  $S^z$  is the  $z$  component of the spin operator, where  $x$ ,  $y$ , and  $z$  are the crystallographic  $a^*$ ,  $b$ , and  $c^*$  axes, respectively.

During the simulation, we verified that neither the dominant exchange interactions,  $J_1$ ,  $J_2$ , and  $J_3$ , nor the

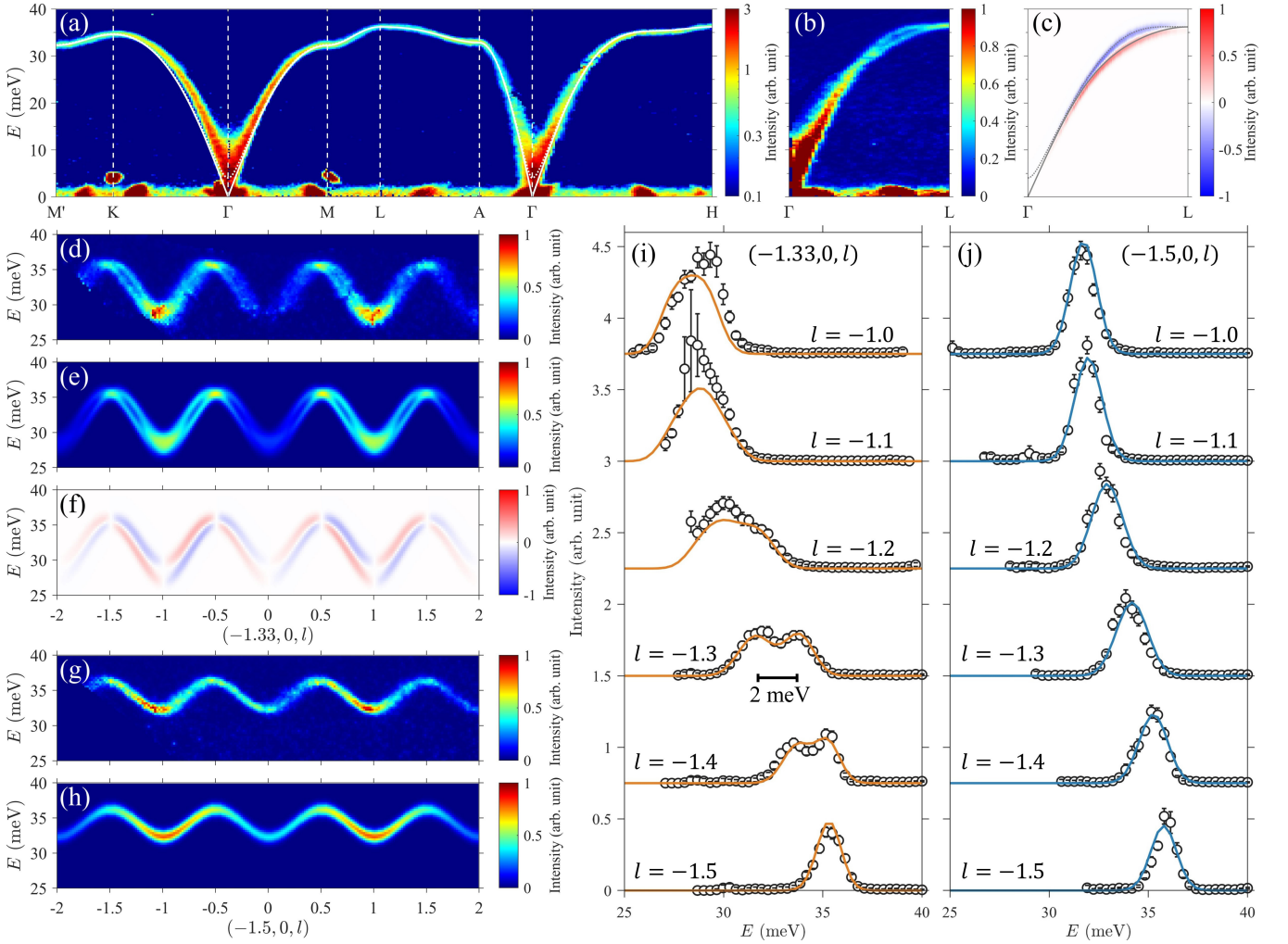


FIG. 2. INS spectra with  $E_i=50.8$  meV at  $T=10$  K and LSWT calculation results. (a) INS spectra along high symmetric  $Q$ -paths inside the spin-degenerate NPs. The colorbar is in logarithm scale. The white solid and dotted curves show two calculated magnon modes. (b) INS spectrum and (c) calculated neutron chiral factor along  $\Gamma - L$  off the spin-degenerate NPs. The gray solid and dotted curves show two calculated magnon modes. (d) INS spectra, (e) calculated neutron structure factor, and (f) calculated neutron chiral factor along  $(-1.33, 0, l)$  off the NPs. (g) INS spectra and (h) calculated neutron structure factor along  $(-1.5, 0, l)$  in the BZ boundary. (i), (j) 1-D constant- $Q$  cuts of the INS spectra and calculated neutron structure factors along  $(-1.33, 0, l)$  and  $(-1.5, 0, l)$ , respectively. The black circles are experimental data and the solid curves are calculations. The  $(-1.33, 0, l)$  and  $(-1.5, 0, l)$  directions correspond to the orange and blue paths shown in Fig. 1(c), respectively.

further forth to ninth nearest neighbor exchange interactions, could explain the split dispersions in Figs. 2(b) and 2(d). The unconventional magnon splitting are irrelevant to relativistic effect as well; Dzyaloshinskii-Moriya interaction is inactive in the centrosymmetric lattice of MnTe, and the single-ion easy-plane anisotropy only lifts the degeneracy near the  $\Gamma$ -point. Thus, the alternating exchange interactions,  $J_{10}$  and  $J_{11}$ , are crucial in the spin Hamiltonian.

Inside the NPs,  $J_1$ ,  $J_2$ ,  $J_3$ ,  $J_{10} + J_{11}$  and  $D$  are the parameters for the dispersion formula. By fitting to the spectra in the NPs by the weighted least squares method, the best solution gives  $J_1 = 3.99(3)$  meV,  $J_2 = -0.120(2)$  meV,  $J_3 = 0.472(3)$  meV,  $J_{10} + J_{11} = 0.0931(8)$  meV and  $D = 0.0482(5)$  meV. The calculated dispersions are

over plotted in Fig. 2(a), suggesting the high consistency. Then, by fitting to the spectra off the NPs, we obtained  $J_{10} = 0.0681(7)$  meV and  $J_{11} = -0.0221(2)$  meV. The calculated neutron structure factors after being convoluted by the instrumental energy resolution are shown in Figs. 2(e) and 2(h). Both the single- and double-peak magnon excitations in Figs. 2(i) and 2(j) are well explained by the obtained spin Hamiltonian. The  $g$ -wave patterns in the constant- $E$  slices are reproduced by the calculations as well, as shown in Figs. 3(d)- 3(f).

To further verify the chirality of the split magnon modes, we calculated the neutron chiral factor based on the obtained spin Hamiltonian by using LSWT. The chi-

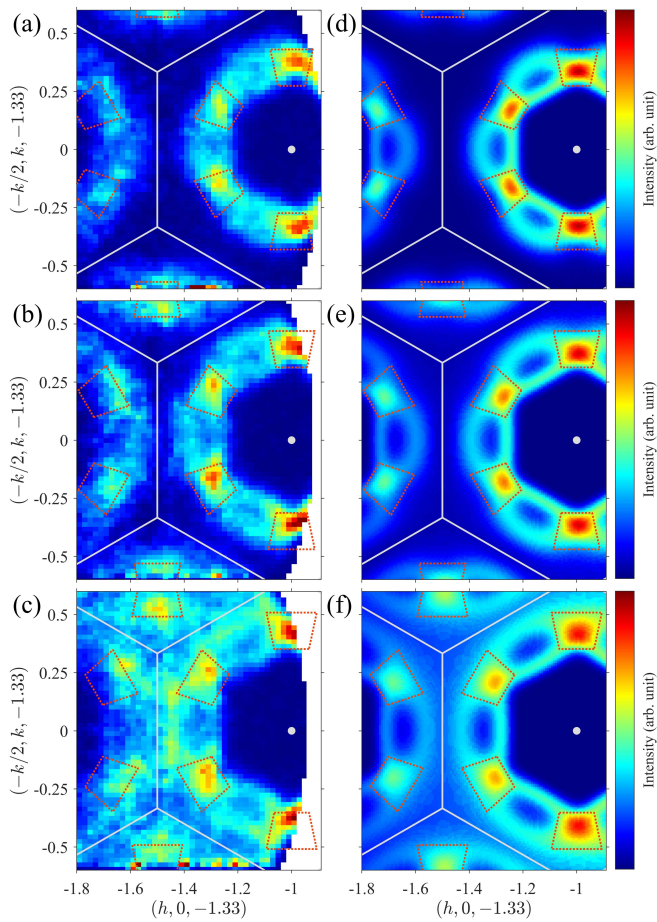


FIG. 3. Constant-energy slices in the  $(h, k, -1.33)$ -plane of (a)  $E = 33$  meV, (b)  $E = 33.5$  meV, and (c)  $E = 34$  meV. (d), (e), (f) LSWT calculations corresponding to (a), (b), and (c). The red dotted trapezoids highlight the six-fold nodal points of the  $g$ -wave contour of the altermagnetic magnon dispersion. The BZs are shown by the solid white lines.

ral factor is represented by

$$M_{\text{ch}} = i(\langle M_Y M_Z^\dagger \rangle - \langle M_Z M_Y^\dagger \rangle), \quad (2)$$

where  $X$  is parallel to  $\mathbf{Q}$ ,  $Y$  is orthogonal to  $X$  in the scattering plane, and  $Z$  is orthogonal to the scattering plane.  $\langle M_\alpha M_\alpha^\dagger \rangle$  ( $\alpha = Y, Z$ ) is the Fourier transform of the spin-spin correlation function. The calculated  $M_{\text{ch}}$  along  $\Gamma - L$  is shown in Fig. 2(c). The magnon modes

split by the altermagnetic exchange interactions exhibit  $M_{\text{ch}}$  with opposite sign, indicating an opposite chirality. Note that  $M_{\text{ch}}$  is zero at the  $\Gamma$ -point. Though the easy-plane anisotropy lifts the two-fold degeneracy of magnon at the  $\Gamma$ -point, the chiral splitting is prohibited here because the TRS is still preserved. Similarly, we plotted  $M_{\text{ch}}$  along  $(-1.33, 0, l)$ , as shown in Fig. 2(f). The alternatively propagating magnon dispersions are alternating chiral-split as well. By contrast, the magnon chirality is completely degenerated and the  $M_{\text{ch}}$  is zero along  $(-1.5, 0, l)$ . These evidence the chiral magnons in a magnet with collinear compensated spin arrangement, in addition to the chiral magnon observed in ferromagnet [43], ferrimagnet [44], and non-collinear  $120^\circ$  antiferromagnet [45].

The identified altermagnetic exchange interactions are different in value and sign, accentuating the distinct spin symmetry of altermagnetism. Though weaker than the dominant interactions in the system by order of magnitude, they bring significant outcomes. As an example, they enable the linear dispersive chiral magnons in altermagnets near the  $\Gamma$ -point, removing the limitation of ferromagnetic magnon spintronics [1]. Also, in addition to the  $s$ -wave ferromagnetism, the altermagnetic exchange interactions lead to  $d, g, i$ -wave magnetic phases, complementing the long missing counterpart of unconventional superconductivity in magnetism [1, 46].

In conclusion, by performing INS measurements, we verified the chiral splitting of magnon in the altermagnet and confirmed the  $g$ -wave magnetism in MnTe. The giant splitting of magnon dispersions reaches 2 meV and is well explained by a pair of alternating exchange interactions. By providing the evidence of altermagnetism from the perspective of spin excitation, this work established a firm foundation for future explorations in this new magnetic phase.

## ACKNOWLEDGMENTS

We are grateful to D. Kawana, T. Asami, and R. Sugiyama for supporting us in the neutron scattering experiment at HRC. The neutron experiment using HRC at the Materials and Life Science Experimental Facility of the J-PARC was performed under a user program (Proposal No. 2024S01). Z. Liu was supported by the Japan Society for the Promotion of Science through the Leading Graduate Schools (MERIT). This project was supported by JSPS KAKENHI Grant Numbers 21H04441.

- 
- [1] L. Šmejkal, J. Sinova, and T. Jungwirth, Emerging research landscape of altermagnetism, *Phys. Rev. X* **12**, 040501 (2022).  
 [2] L. Šmejkal, J. Sinova, and T. Jungwirth, Beyond conventional ferromagnetism and antiferromagnetism: A phase with nonrelativistic spin and crystal rotation symmetry,

- Phys. Rev. X* **12**, 031042 (2022).  
 [3] S. Hayami, Y. Yanagi, and H. Kusunose, Momentum-dependent spin splitting by collinear antiferromagnetic ordering, *J. Phys. Soc. Jpn.* **88**, 123702 (2019).  
 [4] S. Hayami, Y. Yanagi, and H. Kusunose, Bottom-up design of spin-split and reshaped electronic band

- structures in antiferromagnets without spin-orbit coupling: Procedure on the basis of augmented multipoles, *Phys. Rev. B* **102**, 144441 (2020).
- [5] L.-D. Yuan, Z. Wang, J.-W. Luo, E. I. Rashba, and A. Zunger, Giant momentum-dependent spin splitting in centrosymmetric low- $Z$  antiferromagnets, *Phys. Rev. B* **102**, 014422 (2020).
- [6] L.-D. Yuan, Z. Wang, J.-W. Luo, and A. Zunger, Prediction of low- $Z$  collinear and noncollinear antiferromagnetic compounds having momentum-dependent spin splitting even without spin-orbit coupling, *Phys. Rev. Mater.* **5**, 014409 (2021).
- [7] Y. Noda, K. Ohno, and S. Nakamura, Momentum-dependent band spin splitting in semiconducting  $\text{MnO}_2$ : a density functional calculation, *Phys. Chem. Chem. Phys.* **18**, 13294 (2016).
- [8] K.-H. Ahn, A. Hariki, K.-W. Lee, and J. Kuneš, Antiferromagnetism in  $\text{RuO}_2$  as  $d$ -wave pomeranchuk instability, *Phys. Rev. B* **99**, 184432 (2019).
- [9] S. A. Egorov and R. A. Evarestov, Colossal spin splitting in the monolayer of the collinear antiferromagnet  $\text{MnF}_2$ , *J. Phys. Chem. Lett.* **12**, 2363 (2021).
- [10] I. I. Mazin, K. Koepf, M. D. Johannes, R. González-Hernández, and L. Šmejkal, Prediction of unconventional magnetism in doped  $\text{FeSb}_2$ , *Proc. Natl. Acad. Sci.* **118**, e2108924118 (2021).
- [11] Y. Guo, H. Liu, O. Janson, I. C. Fulga, J. van den Brink, and J. I. Facio, Spin-split collinear antiferromagnets: A large-scale *ab-initio* study, *Mater. Today Phys.* **32**, 100991 (2023).
- [12] P. Liu, Y. Wang, H. J. Zhao, L. Bellaiche, and Y. Ma, Magnetically controllable band splittings in  $Pnma$  ferromagnetic materials, *Phys. Rev. B* **105**, 054402 (2022).
- [13] R. Jaeschke-Ubiergo, V. K. Bharadwaj, T. Jungwirth, L. Šmejkal, and J. Sinova, Supercell altermagnets, *Phys. Rev. B* **109**, 094425 (2024).
- [14] J. Krempaský, L. Šmejkal, S. D'Souza, M. Hajlaoui, G. Springholz, K. Uhlířová, F. Alarab, P. C. Constantinou, V. Strocov, D. Usanov, W. R. Pudelko, R. González-Hernández, A. Birk Hellenes, Z. Jansa, H. Reichlová, Z. Šobán, R. D. Gonzalez Betancourt, P. Wadley, J. Sinova, D. Kriegner, J. Minár, J. H. Dil, and T. Jungwirth, Altermagnetic lifting of kramers spin degeneracy, *Nature* **626**, 517 (2024).
- [15] S. Lee, S. Lee, S. Jung, J. Jung, D. Kim, Y. Lee, B. Seok, J. Kim, B. G. Park, L. Šmejkal, C.-J. Kang, and C. Kim, Broken kramers degeneracy in altermagnetic  $\text{MnTe}$ , *Phys. Rev. Lett.* **132**, 036702 (2024).
- [16] T. Osumi, S. Souma, T. Aoyama, K. Yamauchi, A. Honma, K. Nakayama, T. Takahashi, K. Ohgushi, and T. Sato, Observation of a giant band splitting in altermagnetic  $\text{MnTe}$ , *Phys. Rev. B* **109**, 115102 (2024).
- [17] O. Fedchenko, J. Minár, A. Akashdeep, S. W. D'Souza, D. Vasilyev, O. Tkach, L. Odenbreit, Q. Nguyen, D. Kutnyakhov, N. Wind, L. Wenthaus, M. Scholz, K. Rossnagel, M. Hoesch, M. Aeschlimann, B. Stadtmüller, M. Kläui, G. Schönhense, T. Jungwirth, A. B. Hellenes, G. Jakob, L. Šmejkal, J. Sinova, and H.-J. Elmers, Observation of time-reversal symmetry breaking in the band structure of altermagnetic  $\text{RuO}_2$ , *Sci. Adv.* **10**, eadj4883 (2024).
- [18] S. Reimers, L. Odenbreit, L. Šmejkal, V. N. Strocov, P. Constantinou, A. B. Hellenes, R. Jaeschke Ubiergo, W. H. Campos, V. K. Bharadwaj, A. Chakraborty, *et al.*, Direct observation of altermagnetic band splitting in  $\text{CrSb}$  thin films, *Nat. Commun.* **15**, 2116 (2024).
- [19] L. Šmejkal, R. González-Hernández, T. Jungwirth, and J. Sinova, Crystal time-reversal symmetry breaking and spontaneous hall effect in collinear antiferromagnets, *Sci. Adv.* **6**, eaaz8809 (2020).
- [20] L. Šmejkal, A. H. MacDonald, J. Sinova, S. Nakatsuji, and T. Jungwirth, Anomalous hall antiferromagnets, *Nat. Rev. Mater.* **7**, 482 (2022).
- [21] Z. Feng, X. Zhou, L. Šmejkal, L. Wu, Z. Zhu, H. Guo, R. González-Hernández, X. Wang, H. Yan, P. Qin, *et al.*, An anomalous hall effect in altermagnetic ruthenium dioxide, *Nat. Electron.* **5**, 735 (2022).
- [22] R. González-Hernández, L. Šmejkal, K. Výborný, Y. Yahagi, J. Sinova, T. Jungwirth, and J. Železný, Efficient electrical spin splitter based on nonrelativistic collinear antiferromagnetism, *Phys. Rev. Lett.* **126**, 127701 (2021).
- [23] M. Naka, S. Hayami, H. Kusunose, Y. Yanagi, Y. Motome, and H. Seo, Spin current generation in organic antiferromagnets, *Nat. Commun.* **10**, 4305 (2019).
- [24] D.-F. Shao, S.-H. Zhang, M. Li, C.-B. Eom, and E. Y. Tsymlal, Spin-neutral currents for spintronics, *Nat. Commun.* **12**, 7061 (2021).
- [25] H.-Y. Ma, M. Hu, N. Li, J. Liu, W. Yao, J.-F. Jia, and J. Liu, Multifunctional antiferromagnetic materials with giant piezomagnetism and noncollinear spin current, *Nat. Commun.* **12**, 2846 (2021).
- [26] M. Naka, Y. Motome, and H. Seo, Perovskite as a spin current generator, *Phys. Rev. B* **103**, 125114 (2021).
- [27] A. Bose, N. J. Schreiber, R. Jain, D.-F. Shao, H. P. Nair, J. Sun, X. S. Zhang, D. A. Muller, E. Y. Tsymlal, D. G. Schlom, *et al.*, Tilted spin current generated by the collinear antiferromagnet ruthenium dioxide, *Nat. Electron.* **5**, 267 (2022).
- [28] S. Karube, T. Tanaka, D. Sugawara, N. Kadoguchi, M. Kohda, and J. Nitta, Observation of spin-splitting torque in collinear antiferromagnetic  $\text{RuO}_2$ , *Phys. Rev. Lett.* **129**, 137201 (2022).
- [29] H. Bai, L. Han, X. Y. Feng, Y. J. Zhou, R. X. Su, Q. Wang, L. Y. Liao, W. X. Zhu, X. Z. Chen, F. Pan, X. L. Fan, and C. Song, Observation of spin splitting torque in a collinear antiferromagnet  $\text{RuO}_2$ , *Phys. Rev. Lett.* **128**, 197202 (2022).
- [30] A. Hariki, A. Dal Din, O. J. Amin, T. Yamaguchi, A. Badura, D. Kriegner, K. W. Edmonds, R. P. Campion, P. Wadley, D. Backes, L. S. I. Veiga, S. S. Dhesi, G. Springholz, L. Šmejkal, K. Výborný, T. Jungwirth, and J. Kuneš, X-ray magnetic circular dichroism in altermagnetic  $\alpha$ - $\text{MnTe}$ , *Phys. Rev. Lett.* **132**, 176701 (2024).
- [31] T. Aoyama and K. Ohgushi, Piezomagnetic properties in altermagnetic  $\text{MnTe}$ , *Phys. Rev. Mater.* **8**, L041402 (2024).
- [32] L. Šmejkal, A. Marmodoro, K.-H. Ahn, R. González-Hernández, I. Turek, S. Mankovsky, H. Ebert, S. W. D'Souza, O. Šipr, J. Sinova, and T. Jungwirth, Chiral magnons in altermagnetic  $\text{RuO}_2$ , *Phys. Rev. Lett.* **131**, 256703 (2023).
- [33] T. A. Maier and S. Okamoto, Weak-coupling theory of neutron scattering as a probe of altermagnetism, *Phys. Rev. B* **108**, L100402 (2023).
- [34] J. E. D'Sa, P. Bhoje, K. Priolkar, A. Das, S. Paranjpe, R. Prabhu, and P. Sarode, Low-temperature neutron diffraction study of  $\text{MnTe}$ ,

- J. Magn. Magn. Mater. **285**, 267 (2005).
- [35] W. Szuszkiewicz, B. Hennion, B. Witkowska, E. Lusakowska, and A. Mycielski, Neutron scattering study of structural and magnetic properties of hexagonal MnTe, *Phys. Status Solidi C* **2**, 1141 (2005).
- [36] D. Krieger, H. Reichlova, J. Grenzer, W. Schmidt, E. Ressouche, J. Godinho, T. Wagner, S. Y. Martin, A. B. Shick, V. V. Volobuev, G. Springholz, V. Holý, J. Wunderlich, T. Jungwirth, and K. Výborný, Magnetic anisotropy in antiferromagnetic hexagonal MnTe, *Phys. Rev. B* **96**, 214418 (2017).
- [37] W. Szuszkiewicz, E. Dynowska, B. Witkowska, and B. Hennion, Spin-wave measurements on hexagonal MnTe of NiAs-type structure by inelastic neutron scattering, *Phys. Rev. B* **73**, 104403 (2006).
- [38] D. Mateika, Growth of MnTe single crystals from nonstoichiometric melts by liquid encapsulation, *J. Cryst. Growth* **13**, 698 (1972).
- [39] S. Itoh, T. Yokoo, S. Satoh, S. ichiro Yano, D. Kawana, J. Suzuki, and T. J. Sato, High resolution chopper spectrometer (HRC) at J-PARC, *Nucl. Instrum. Meth. A* **631**, 90 (2011).
- [40] S. Itoh, T. Yokoo, T. Masuda, S. Asai, H. Saito, D. Kawana, R. Sugiura, T. Asami, and Y. Ihata, Progress in high resolution chopper spectrometer HRC by improving collimator and Fermi chopper, *Physica B Condens. Matter* **568**, 76 (2019).
- [41] D. Kawana, M. Soda, M. Yoshida, Y. Ikeda, T. Asami, R. Sugiura, H. Yoshizawa, T. Masuda, T. Hawai, S. Ibuka, T. Yokoo, and S. Itoh, YUI and HANA: Control and visualization programs for HRC in J-PARC, *J. Phys. Conf. Ser.* **1021**, 012014 (2018).
- [42] S. Toth and B. Lake, Linear spin wave theory for single- $Q$  incommensurate magnetic structures, *J. Condens. Matter Phys.* **27**, 166002 (2015).
- [43] K. Jenni, S. Kunkemöller, W. Schmidt, P. Steffens, A. A. Nugroho, and M. Braden, Chirality of magnetic excitations in ferromagnetic SrRuO<sub>3</sub>, *Phys. Rev. B* **105**, L180408 (2022).
- [44] Y. Nambu, J. Barker, Y. Okino, T. Kikkawa, Y. Shiomi, M. Enderle, T. Weber, B. Winn, M. Graves-Brook, J. M. Tranquada, T. Ziman, M. Fujita, G. E. W. Bauer, E. Saitoh, and K. Kakurai, Observation of magnon polarization, *Phys. Rev. Lett.* **125**, 027201 (2020).
- [45] M. Loire, V. Simonet, S. Petit, K. Marty, P. Bordet, P. Lejay, J. Ollivier, M. Enderle, P. Steffens, E. Ressouche, A. Zorko, and R. Ballou, Parity-broken chiral spin dynamics in Ba<sub>3</sub>NbFe<sub>3</sub>Si<sub>2</sub>O<sub>14</sub>, *Phys. Rev. Lett.* **106**, 207201 (2011).
- [46] D. Zhu, Z.-Y. Zhuang, Z. Wu, and Z. Yan, Topological superconductivity in two-dimensional altermagnetic metals, *Phys. Rev. B* **108**, 184505 (2023).